Electrochemical synthesis of 2D copper coordination-polymers: Layer-stacking deviation induced by the solvent and its effect on the adsorptive properties

Arthur Felipe de Farias Monteiro [a], Stephany Larissa da Silva Ribeiro [b],
Thiago Izidoro Silva Santos [c], José Daniel da Silva Fonseca [a], Natalia Łukasik [d,e],
Joanna Kulesza [a,**], Bráulio Silva Barros [f,*]

[a] Departamento de Química Fundamental, Universidade Federal de Pernambuco, Av. Prof. Moraes Rego, 1235 - Cidade Universitária, 50670-901, Recife, PE, Brazil
[b] Instituto de Química, Universidade Federal de Goiás, Campus Samambaia, 74690-900, Goiânia, GO, Brazil
[c] Departamento de Química, Universidade Federal de São Carlos, Rodovia Washington Luis s/n Km 235, 13565-905, São Carlos, SP, Brazil
[d] Programa de Pós-graduação em Química, Universidade Federal de Pernambuco, Av. Prof. Moraes Rego, 1235 - Cidade Universitária, 50670-901, Recife, PE, Brazil
[e] Department of Chemistry and Technology of Functional Materials, Faculty of Chemistry, Gdansk University of Technology, 11/12 Narutowicza Street, 80-233, Gdansk, Poland
[f] Departamento de Engenharia Mecânica, Universidade Federal de Pernambuco, Av. Prof. Moraes Rego, 1235 - Cidade Universitária, 50670-901, Recife, PE, Brazil

ARTICLE INFO

ABSTRACT

A 2D Cu-based Metal-Organic Framework (MOF), namely copper-terephthalate (Cu(1,4-BDC)), was successfully synthesized by electrochemical method for effective methylene blue (MB) sorption from aqueous solutions. The composition, morphology, and the presence of functional groups in the obtained material were verified by Fourier Transform Infrared spectroscopy (FTIR), Powder X-Ray Diffraction (PXRD), Thermal (TGA), and Elemental (EA) analysis, as well as Scanning Electron Microscopy (SEM). The effect of electrochemical parameters applied in the synthesis protocol (i.e., a potentiometric or amperometric mode) on the resulting product composition was evaluated. The electric current value was determined as a variable controlling the type of crystal structure present in the obtained MOF. A structure with open channels - CuBDC1 was favored under the current higher than 0.35 A conditions. In contrast, for the lower current values and upon the amperometric mode in the material, a CuBDC2 phase with DMF molecules occupying the grids of the layers was also present. The MB sorption studies were analyzed both with kinetic and equilibrium models. The obtained results showed the time evolution could be fitted with a pseudo-second-order model with the rate constant k_2 equal to 0.047 g μmol^{-1} h^{-1}. According to the Langmuir isotherm model, the maximum sorption capacity was determined as 76.63 μmol g^{-1}. After MB sorption, the MOF material could be easily regenerated under mild conditions with good recyclability up to the four cycles (76.77%).

1. Introduction

Layered Metal-Organic Frameworks (2D-MOFs) have received much attention in the past years due to their unique set of properties, which includes a structure with the presence of open, active sites, permanent porosity, and high surface area. 2D-MOFs are formed by stacking layers with a metal-organic structure held by strong coordination bonds. In contrast, the forces between the layers are weak, typically hydrogen bonding, π–π stacking, and other supramolecular interactions. Such frameworks meet many possible uses in energy and environmental-related applications such as catalysis, sensing, adsorption, and separation [1–4]. Furthermore, 2D-MOFs have already shown better performance than 3D-MOFs for several applications, such as dye adsorption, which can be explained by the improved diffusion and better access to the active sites within the structure [5,6].

Copper-based MOFs such as the Cu(1,4BDC) may crystallize with a

---

2D layered structure. The building block unit is based on a paddle-wheel type binuclear cluster coordinated by four 1,4-BDC[2-] anions in a bidentate bridging mode, which leads to the formation of uniform square-grid layers. Besides, each copper ion of the cluster is also coordinated by one solvent molecule, such as water, ethanol, DMF, etc. [7,8]. The stacking of these square-grid layers gives rise to 1D infinite channels within each layer [6]. Interestingly, changing the type of solvent may induce deviation in the stacking order of the 2D layers leading to changes in the porosity of the framework [7]. As reported, the conventional synthesis methods lead to the stacking of square-grid layers shifted relative to each other, showing a low symmetry, typically P2 or C2. In comparison, using a liquid phase epitaxy method leads to the packing of layers with P4 symmetry [9–12]. Most importantly, by changing the symmetry of the stacking, it is possible to increase the free space within the 1D channels observed in this kind of structure and its adsorption capacity for organic compounds.

Indeed, due to their porous structure, MOFs are considered an innovative platform for developing new sorbents for organic dyes in aqueous media. The presence in natural water systems of diverse colorants coming from, among others, textiles, food, plastic, and cosmetics industries poses a serious ecological threat. Even at low concentrations, dyes reduce water quality significantly, decreasing the oxygen solubility and light penetration in water, influencing photosynthesis and functions of aquatic organisms [13,14]. Many synthetic dyes reveal toxic, mutagenic, and carcinogenic properties, and some, due to their complex structure, are resistant to oxidizing agents and biodegradation [15,16]. Thus the development of efficient, relatively simple, and economical methods of eliminating dyes from waters without the generation of secondary pollutants is highly demanded. To this date, several pristine or modified MOFs have been successfully tested for the removal of dyes. Lin and co-workers [17] reported that HKUST-1, a well-known Cu-BTC-based MOF, possesses great potential for removing the cationic dye – methylene blue (MB) from wastewater through adsorption. The incorporation of TiO_2 nanoparticles on the surface of HKUST-1 ensured MB removal by synergic adsorption and photocatalytic degradation upon irradiation with visible light [18]. For the structural analog of HKUST-1, derived from benzene-1,2,4-tricarboxylic acid, even better sorption efficiency was described, indicating how important it is to determine the relationship between molecular structure and sorption properties of the materials [19]. Haque and co-workers [20] verified the effect of the electrostatic forces on the dye adsorption capacity of an iron terephthalate (MOF-235). The authors used methylene blue (MB) and methyl orange (MO) as representative cationic and anionic dyes, respectively. The adsorption of MB and MO at different temperatures on the MOF-235 was tested, and the results indicated a spontaneous and endothermic process that allowed a much higher adsorption capacity than those observed for activated carbon. The highly porous metal-organic framework MIL-101 was used to adsorb xylenol orange (XO) from an aqueous solution [21]. This chromium-benzenedicarboxylate showed a high adsorption capability compared to other well-known adsorbents like active carbon and MCM-41, especially under low pH conditions. Recently, a two-dimensional Cu(II)-5-azidoisophthalate MOF was applied to the adsorption of methylene blue (MB), rhodamine B (RhB), methyl orange (MO), and congo red (CR) [6]. It was found that the adsorption is dependent on the shape, dimension, and ionic strengths of the adsorbate, in this case, the organic dyes. According to the authors, this 2D MOF possesses an anionic nature and is a more efficient adsorbent than its analogous 3D or 0D materials. Au et al. [22] described Cu-MOFs obtained from di- and tri-topic carboxylate linkers derived from 2,4,6-triphenylpyridine as materials of dual functionality in removal of organic dyes. The cationic dyes, MB and malachite green (MG), were effectively adsorbed by the materials, whereas an anionic dye – tartrazine was degraded in a photo-Fenton-like reaction catalyzed by the MOFs-H_2O_2 systems under irradiation with visible light.

In this paper, we report the electrochemical synthesis of a copper-based 2D MOF and its application in organic dye adsorption using methylene blue as a model adsorbate. Although the material has already been described in the literature, to the best of our knowledge, its sorption effectiveness towards organic dyes was not investigated so far. We have studied the solvent-induced deviation in the stacking of the square-grid layers and its effect on the dye adsorption capability of the produced samples. Additionally, synthetic parameters like voltage and current were also investigated. While the conventional solvothermal method requires several hours of synthesis, the products in the electrochemical procedure can be obtained after 1 h. The detailed studies of the influence of parameters of the synthetic protocol on the material composition and resulting sorption properties may be a significant step in developing effective and recyclable MOF-based sorbents representing an alternative to the activated carbons commonly used in the industry.

2. Experimental

2.1. Materials

Terephthalic acid (1,4-H_2BDC, 98%) was purchased from Sigma-Aldrich Co. (USA). Copper wires were acquired from JFPasqua (3.26 mm, $\geq$ 99%), sodium nitrate ($NaNO_3$, >98%) was purchased from Vetec Ltd. (BRA), *N,N*-dimethylformamide (DMF, > 99%), ethanol (99,5%) and methylene blue (MB, > 98%) were purchased from Neon (BRA), Jalles Machado S/A (BRA) and Labsynth (BRA), respectively. All chemicals were used as obtained from commercial sources without further purification.

2.2. Synthesis

Cu-BDC MOFs were synthesized by an electrochemical method reported previously by Martinez Joaristi [23]. In a typical procedure, 1,4-H_2BDC (1.0 g) and sodium nitrate (0.60 g) were dissolved in a water/DMF mixture (80 mL, 1:1 vol). Two copper wires were used as electrodes and inserted into the solution; then, a potential difference was applied to oxidize the copper. The synthesis was managed in potentiometric and amperometric modes. In the first mode, the current was varied from 0.1 to 0.5 A in steps of 0.1 A, and the voltage was measured (samples A1-A6). For the amperometric mode, the voltage was varied from 7 to 12 V in steps of 1 V, and the current was measured (samples B1–B6). The solution was kept under magnetic stirring for 1 h, then the solid was recovered by centrifugation and washed with DMF and water three times each, respectively. The solid was dried at 60 °C for 3 h, and finally, the products were obtained as a dry powder.

2.3. Characterization

The as-obtained products were analyzed by X-ray powder diffraction (PXRD) on a Bruker D2 Phaser diffractometer using CuKα radiation (λ = 1.5406 Å) in the range from 5° to 50°. The PXRD patterns and hypothetical structures were visualized by Mercury 4.2.0 [24] and Diamond 4.6.6 [25] software. Fourier transform infrared spectra were recorded on a Bruker FTIR – Vertex 70 spectrometer in the range from 4000 to 400 cm^{-1}. The morphology of synthesized samples was observed by Scanning Electron Microscopy (SEM) in a Quanta 200 FEG equipment. Thermogravimetric analysis (TGA) was performed on a Shimadzu DTG-60H. The samples were heated from 25 °C to 600 °C at a rate of 5 °C/min under a nitrogen atmosphere (100 mL/min). Elemental analysis was obtained on a PerkinElmer 2400 Series II CHN elemental analyzer. Sample A5 was characterized for its pore properties by nitrogen adsorption/desorption at the temperature of liquid nitrogen (77.3 K) in a Quantachrome NovaWin2 adsorption apparatus. The surface area of the sample was determined by BET and BJH models. Before the measurement, the sample was degassed at 180 °C for 3 h.

2.4. Adsorption experiments

An accurately weighed quantity of the dye was dissolved in distilled water to prepare the stock solution (250 mg L^{-1}). Experimental solutions of the desired concentrations were obtained by successive dilutions. Due to the high absorptivity of the dye, the initial and most of the final solutions (after adsorption) were properly diluted to obtain a well measurable absorption. The dye concentration was determined in triplicate by UV–Vis spectroscopy performed on an EVEN IL-592 spectrophotometer. The wavelength used for the measurements was 665 nm, related to the band of the maximum absorbance of methylene blue [17,20].

The influence of pH, sorbent dosage, dye concentration, temperature, and contact time on the adsorption capacity was studied.

For the pH experiments, the maximum adsorption capacity was determined using Cu-BDC1 (30 mg) dispersed in a stock solution (20 mL) of MB (250 mg L^{-1}) under stirring for 14 h at a temperature of 20 °C. For the stock solution, pH was adjusted from 2.0 to 12.0 using HCl (0.1 mol L^{-1}) or NaOH (0.1 mol L^{-1}) solutions. The experiments were conducted in triplicate for each pH value to determine the best dye adsorption conditions. To calculate the dye uptake following equation was used:

$$Q_e = \frac{(C_0 - C_e)V}{mM} \tag{1}$$

where Q_e (mmol g^{-1}) is the amount of the dye adsorbed per gram of the sorbent, C_0 and C_e (mg L^{-1}) are MB concentrations before and after sorption, M (g mol^{-1}) is the MB molar mass, V (L) is a volume of the used MB solution, and m is a mass of the sorbent (g).

The sorbent dosage on the adsorptive capacity of the material CuBDC1 was also studied. The experiments were carried out at 20 °C by changing the quantity of sorbent (10, 30, 50, and 100 mg) in the test solution while maintaining the initial dye concentration at 100 mg L^{-1}, contact time of 5 h, and pH of 5.5.

In classic adsorption kinetic studies, Cu-BDC (50 mg) was dispersed in the stock solution (50 mL); after, the mixture was stirred for 7 h. The dye concentration was monitored at the following intervals: 0.5, 1.0, 2.0, 3.0, 5.0, and 7 h, finally. The tests were performed for different methylene blue initial concentrations (25, 50, 100, 150, 200, and 250 mg L^{-1}) and temperatures (20, 30, and 40 °C). In all cases, data were obtained from 1 mL aliquot at each evaluation, collected for the dilution 1:4 for each monitoring. To investigate the kinetic behavior of MB, the linear pseudo-first (eq. (2)) [26] and pseudo-second (eq. (3)) [27] order kinetic models were used:

$$ln\,(Q_e - Q_t) = ln\,Q_e - k_1 t \tag{2}$$

$$\frac{t}{Q_t} = \frac{1}{k_2 Q_e^2} + \frac{t}{Q_e} \tag{3}$$

where Q_e and Q_t (mmol g^{-1}) are adsorption capacities at equilibrium and at a time t (h), respectively, and k_1 (h^{-1}) and k_2 (g $mmol^{-1}$ h^{-1}) are the rate constants of pseudo-first and pseudo-second order models, respectively.

Using parameters obtained from equation (3), the half-life time ($t_{1/2}$) and the initial adsorption rate (h) can be calculated according to the following equations (4) and (5):

$$t_{\frac{1}{2}} = k_2 Q_e^2 \tag{4}$$

$$h = \frac{1}{k_2 Q_e} \tag{5}$$

The values of activation energy, E_a, and the behavior of the kinetic constant against temperature were evaluated using an Arrhenius equation (6):

$$k_2 = Ae^{-\frac{Ea}{RT}} \tag{6}$$

Additionally, the intraparticle diffusion model expressed by the following equation was examined:

$$Q_t = k_i t^{1/2} + C \tag{7}$$

where Q_t (mmol g^{-1}) is the amount of the solute at the surface of the adsorbent at a time t (h), k_i (mmol g^{-1} $h^{-0.5}$) is the constant of intraparticle diffusion rate, and C (mmol g^{-1}) is an intercept [28].

In isothermal adsorption studies, the same conditions as in kinetic studies were used; however, the contact time between MB and the sorbent was set as 7 h. The Langmuir and Freundlich equations were applied to fit the adsorption isotherm.

The Langmuir model is based on assumptions that a sorbent surface has a fixed number of energetically homogeneous adsorption sites and that upon the adsorption, a reversible monolayer is created, in which adsorbate species interact exclusively with the pores and not with each other [29,30]. The model can be described by equation (8) with its linearized form (equation (9)):

$$Q_e = \frac{K_L Q_m C_e}{1 + K_L C_e} \tag{8}$$

$$\frac{C_e}{Q_e} = \frac{1}{Q_m K_L} + \frac{C_e}{Q_m} \tag{9}$$

where K_L is the Langmuir constant, and Q_m is the maximum amount of solute adsorbed on the 1 g of the material surface.

The equilibrium parameter R_L was determined according to equation (10):

$$R_L = \frac{1}{1 + C_m K_L} \tag{10}$$

Where C_m is the initial maximum concentration of adsorbate. The Langmuir constant estimates how favorable this adsorption process is. Its value can vary from 0 to 1 for favorable processes. Values above 1.0 indicate poor propensity. The Freundlich isotherm is based on the assumption that an adsorption process takes place on heterogeneous surfaces, which means the adsorption sites are not energetically identical [30,31]. The model is expressed by the following equation (11) and its linear form (12):

$$Q_e = K_F C_e^{\frac{1}{n}} \tag{11}$$

$$lnQ_e = lnK_F + \left(\frac{1}{n}\right)lnC_e \tag{12}$$

where K_F is the Freundlich constant and $1/n$ is the heterogeneity constant.

The thermodynamic parameters of the sorption process were calculated from the following equations:

$$\Delta G = -RTlnK \tag{13}$$

$$\Delta G = \Delta H - T\Delta S \tag{14}$$

where ΔG, ΔS, and ΔH are Gibbs free energy, entropy, and enthalpy change, respectively, K is a constant determined from the best-fitted isotherm.

The material renewability was tested under optimized pH (5.5) and temperature (20 °C) conditions. The material (40 mg) was dispersed in the dye stock solution (20 mL, 250 mg L^{-1}) and kept for 14 h. The dye desorption was performed by washing the material with a portion of ethanol (10 mL, 99.5%). Five adsorption/desorption cycles were performed.

For real water applications, the model MB solution (c = 100 mg L^{-1}) was prepared using water from a natural reservoir in the metropolitan region of Recife. The sorption material (50 mg) was dispersed in 20 mL of the dye solution and stirred for 5 h at 20 °C. After that time, the phases

were separated by centrifugation, and the solutions were analyzed by UV–Vis spectrophotometry.

3. Results and discussion

3.1. Study of the electrochemical parameters

One of the most significant advantages of the electrochemical synthesis method is to allow the control of the synthetic rate via electrochemical means. In the synthesis of MOFs, the anodic dissolution of the electrode provides the metal ions to a precursor mixture containing the organic linker (terephthalic acid) and an electrolyte (sodium nitrate). Thus, the dissolution rate of the electrode controls the synthesis rate. Both potentiometric (fixed current) and amperometric (fixed voltage) modes were used to study the effects of the anodic dissolution of copper electrodes and their role in the crystallization of Cu-MOFs. In Fig. 1, the profiles of current and voltage as a function of time are shown.

Potentiometric experiments were carried out by applying a fixed current from 0.1 to 0.5 A for 60 min while the voltage between the electrodes was measured (Fig. 1a). The voltage remained practically constant during the synthesis when a low current value was used (0.1–0.2 A), while it decreased significantly when a higher current was applied (0.3–0.5 A). It is worth mentioning that in an electrochemical cell, current and voltage are related to a third electrical quantity, the resistance, through Ohm's law (Eq. (15)).

$$V = R*I \tag{15}$$

where V is the voltage, R is the resistance of the medium, and I is the electric current.

The variations in the voltage measured between the electrodes indicate changes in the resistance of the medium, which in turn corresponds to the inverse of the conductivity. Based on Ohm's law, it can be concluded that at higher fixed-current values, the resistance decreases, or, in other words, the ionic conductivity of the medium rises along the
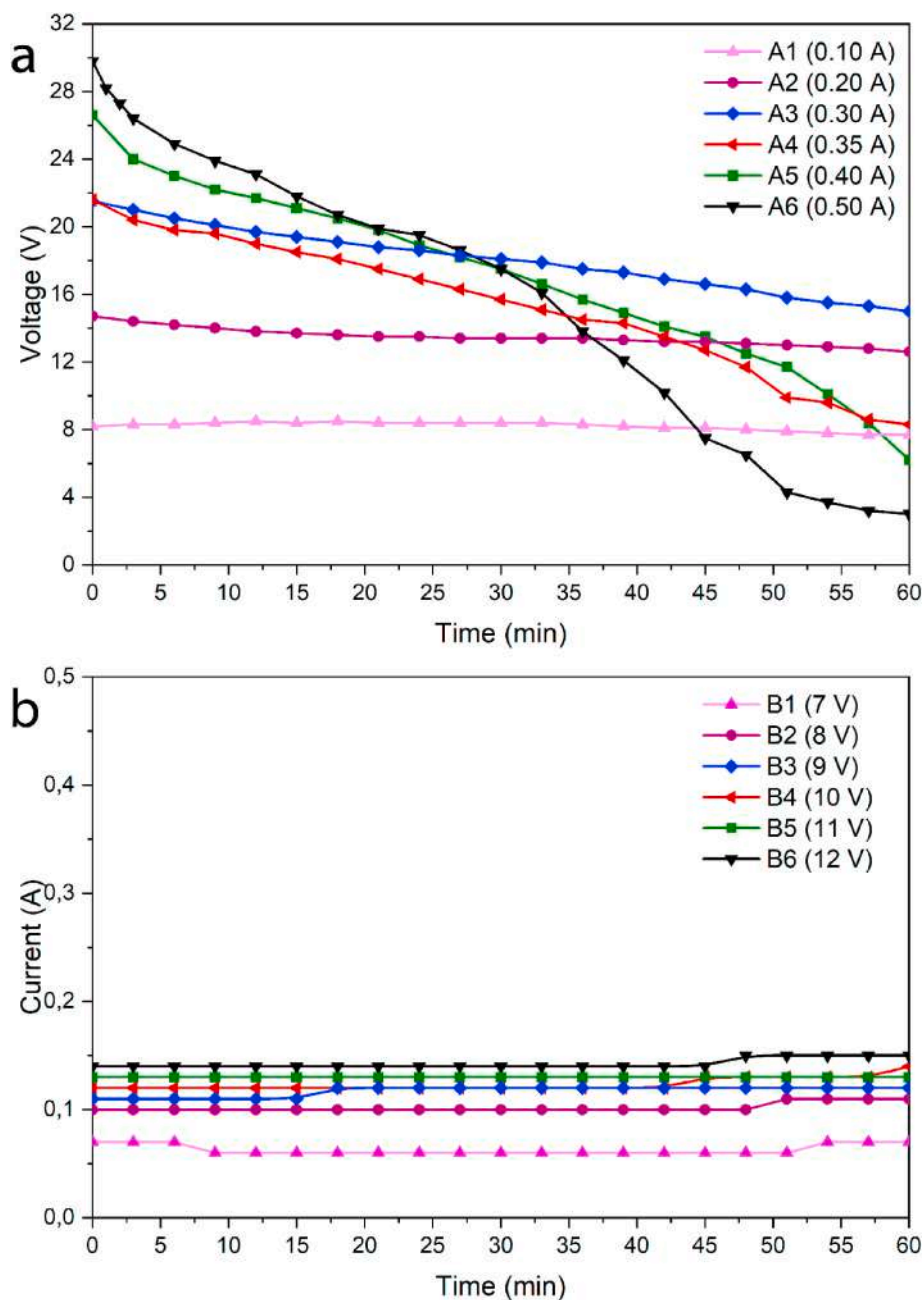

Fig. 1. Variation of electrical (a) current and (b) voltage in the electrochemical cell during the synthesis of the Cu-MOFs.

reaction time. This is consistent with the fact that the concentration of ionized chemical species increases over the reaction time. The electric current corresponds to the quantity of charge flowing per time unit. In an electrochemical reaction, the higher the number of charges, the greater the concentration of ionized chemical species. Therefore, the higher is the electric current, the higher is the concentration of copper ions and carboxylate groups in the medium, this last one formed by deprotonation of the ligand. Indeed, this can explain the most accentuated drop in voltage during the synthesis of samples A4-A6.

The synthesis yield varied from 60 to 80% for samples from A1 to A6, respectively. This is a clear indication that by increasing the electric current, it is possible to increase the number of copper ions in the solution and so the rate of synthesis. Moreover, it is also possible to control the metal/ligand ratio during the reaction, a synthetic parameter that plays an essential role in the crystallization, structure, and morphology of MOFs [32,33].

The experiments performed in the amperometric mode were carried out by applying a fixed voltage from 7 to 12 V for 60 min while the current passing through the electrodes was measured (Fig. 1b). Contrary to what was observed in the potentiometric mode, the electrical quantity monitored (current) did not show any significant changes over the synthesis time, remaining below 0.2 A during all experiments. However, it is worth pointing out that in the case of sample B1, the measured current was lower than 0.08 A. It appears that the electrochemical synthesis of Cu-MOFs is much more sensitive to the electric current than the voltage applied.

3.2. FTIR analysis

FTIR spectra of the samples prepared under constant current A1-A6 and constant voltage B1–B6 compared to the spectra of the ligand 1,4-H_2BDC and the solvent DMF are shown in Fig. 2a and b, respectively. The samples A4-A6 present similar spectra with the intense bands at 1571 and 1394 cm^{-1} attributed, respectively, to the stretching, asymmetric (ν_{as}), and symmetric (ν_s) vibrations of the COO$^-$ groups [34,35]. The difference between (ν_{as}) and (ν_s), equal to $\Delta\nu = 177$ cm^{-1}, might
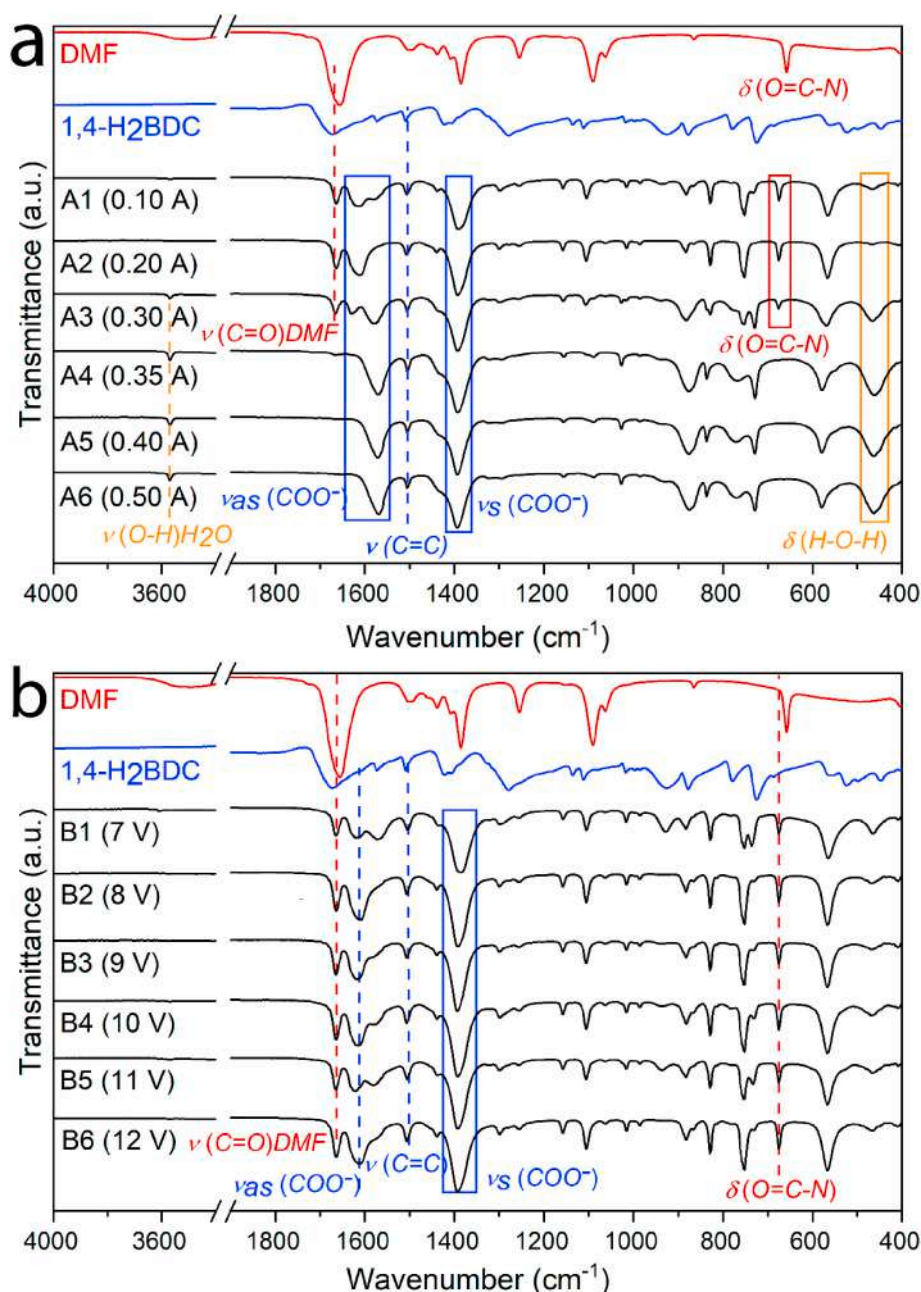

Fig. 2. FTIR spectra of the samples prepared under constant (a) current and (b) voltage compared to the spectra of the ligand 1,4-H_2BDC and DMF.

indicate a bridging bidentate coordination mode of carboxylates [36, 37]. Analyzing the spectra of samples A1-A3, one can observe the presence of an additional band in comparison to the spectra of A4-A6, with the most significant one located at 1610 cm^{-1} assigned to the ν_{as} (COO$^-$) vibrations which may indicate the presence of a secondary phase in these samples. The bands at 3567 and 465 cm^{-1} may suggest the presence of coordinated water molecules in the structure of samples A3-A6. Moreover, the bands at 1672 and 675 cm^{-1} may be attributed to the stretching ν (C=O) and bending δ (OCN) vibrations of the coordinated DMF molecules (A1-A3) [10]. The presence of DMF molecules coordinated to the copper centers should alter the strength of COO–Cu bonds and, consequently, the vibrations of COO$^-$ groups. The higher $\Delta\nu$ = 216 cm^{-1} compared to $\Delta\nu$ = 177 cm^{-1} (found for samples A4-A6) may also indicate the coordination of the DMF molecules to the copper sites.

The spectra of the samples prepared under constant voltage (Fig. 2b) consist of the same bands for all samples (B1–B6), with the most significant ones at 1610, 1571, and 1394 cm^{-1}, corresponding to the stretching, asymmetric (ν_{as}) and symmetric (ν_s) vibrations of the COO$^-$ groups, respectively. The increased number of the asymmetric COO$^-$

bands indicates more than one coordination mode, suggesting the presence of a mixture of phases. The same bands were found for the samples prepared under constant current (for lower current values A1-A3), for which the mixture of phases was also observed. All samples B1–B6 contain probably coordinated DMF molecules in the structure as the samples prepared under constant current (A1-A3).

3.3. PXRD analysis

The powder X-ray diffraction patterns of the samples synthesized with a fixed electric current are shown in Fig. 3a. The diffraction patterns of samples A1 and A2 are in good agreement with that calculated from the crystal structure of Cu(1,4-BDC)(DMF) (CCDC deposition number 687690), here named CuBDC2. However, a low-intensity peak observed at 8.5° suggests the presence of a secondary phase. It is possible to find the same peak in the diffraction patterns obtained for the samples A3–A6, but this time with high intensity. Indeed, this crystalline phase appears in sample A3 together with CuBDC2, while it seems to be the only phase present in samples A4–A6.
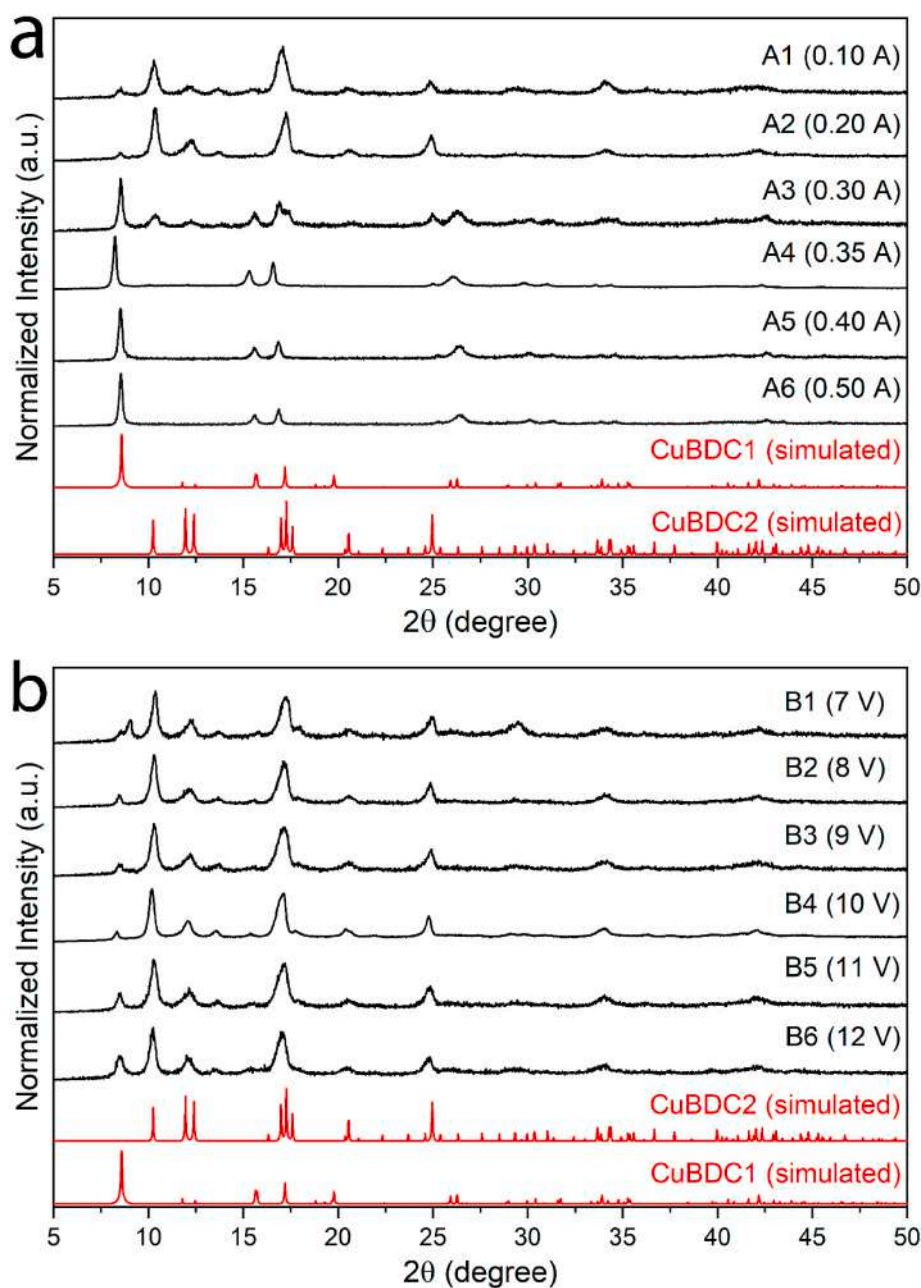

Fig. 3. PXRD patterns of the samples prepared under constant (a) current and (b) voltage compared to the simulated patterns of MOFs CuBDC1 and CuBDC2.
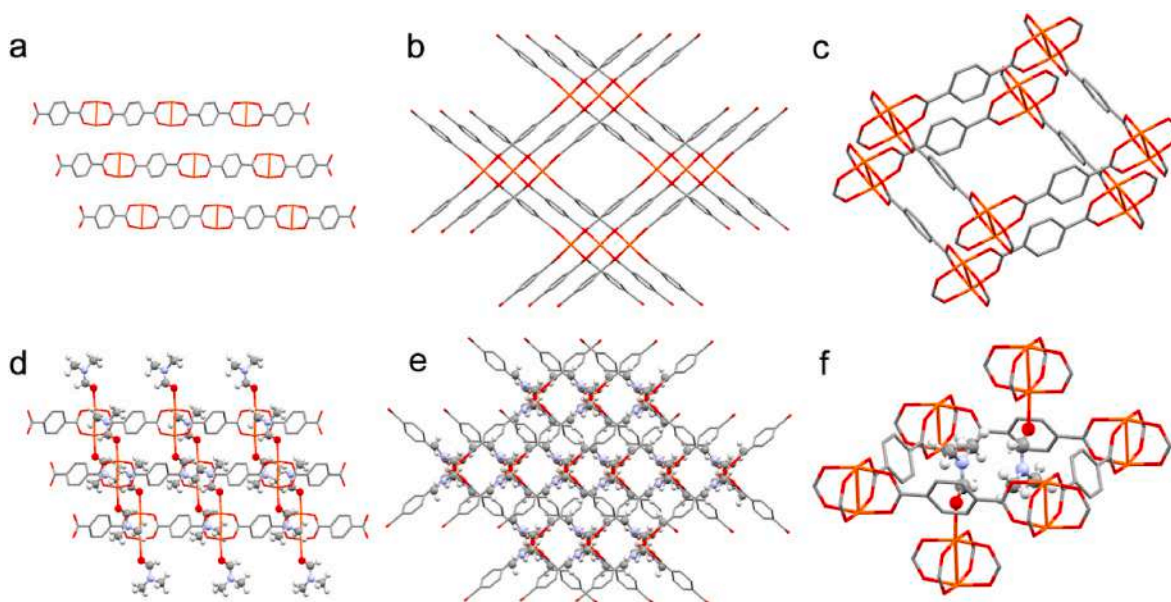
Fig. 4. Schematic representation of the layered structures of (a–c) CuBDC1 (water molecules omitted for clarity) and (d–f) CuBDC2. The schemes emphasize the layer stacking shift due to the presence of different solvent-types coordinated to copper atoms at the apical positions of paddle-wheel clusters. Hydrogen atoms in MOFs are omitted for the clarity of the figures. Color coding: red = oxygen, gray = carbon, blue = nitrogen, white = hydrogen. (For interpretation of the references to color in this figure legend, the reader is referred to the Web version of this article.)

Despite efforts made to identify this crystalline phase using both the Cambridge Structural Database (CSD) and the Crystallography Open Database (COD), no satisfactory match was reached. However, similar diffraction patterns of Cu(1,4-BDC) MOFs were previously reported by Liu et al. [12], Arslan et al. [38], and our group [39]. Based on the information given by these authors, the expected composition, and a careful search in the CSD for related frameworks, a hypothetical crystalline structure was proposed. Thus, the crystal structure of the Cu-MOF assembled with DMTA (2,5-imethoxyterephthalic acid) reported by Guo and co-workers [40] was used as a template. The crystallographic information available in the corresponding cif file (CCDC deposition number 898032) was conveniently modified and used to generate a hypothetical structure named here CuBDC1. The whole procedure is described in the support information section. The diffraction patterns of the samples A4–A6 are in good agreement with the calculated pattern of the hypothetical structure, while sample A3 presents a mix of the phases CuBDC1 and CuBDC2. A comparative analysis of the phases observed in the diffraction patterns suggests that higher electric currents starting from 0.35 A favor the crystallization of the phase CuBDC1.

The X-ray diffraction patterns of the samples prepared at constant voltage are shown in Fig. 3b. As can be seen, all samples present the main phase CuBDC2 and the secondary phase CuBDC1. These results are consistent with those obtained from the samples prepared in the potentiometric mode, indicating that the electric current is the variable that determines the type of crystal structure formed in the final product.

Although CuBDC1 and CuBDC2 show a distinct set of characteristic diffraction peaks, they both crystallize in the monoclinic space group C2/m and present a layered structure, as displayed in Fig. 4. These MOFs show a square grid structure formed by paddle-wheel Cu_2 clusters connected through four molecules of 1,4-BDC along two dimensions. Furthermore, the paddle-wheel clusters may be coordinated in their apical positions by solvent molecules like DMF (CuBDC2). The structure proposed for CuBDC1 does not consider the presence of solvent molecules. However, they may be present in the channels. The absence of coordinated solvent molecules reduces the displacement between layers, originating a 3D framework with empty channels across the vertical direction (see Fig. 4b and c). On the other hand, in CuBDC2, the apical positions of the clusters are coordinated by DMF molecules. These bulky
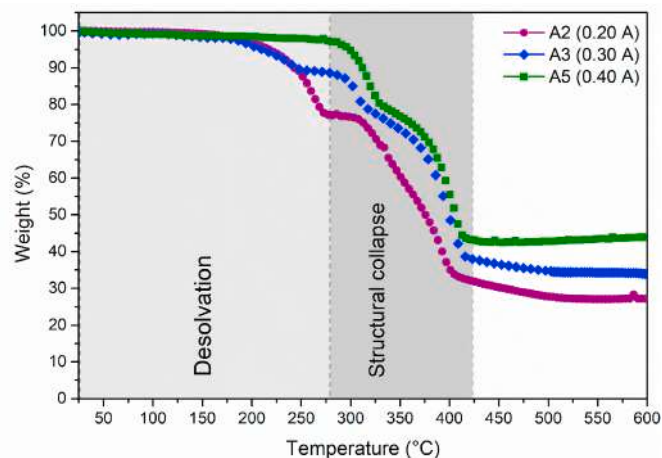

Fig. 5. Thermogravimetric curves of samples A2, A3, and A5.

molecules tend to occupy the grids of the layers, making the volume of the channels not available (see Fig. 4d and f). Apparently, in this case, the stacking of layers is held by weak interactions between DMF molecules or aromatic rings.

3.4. Thermal and elemental analysis

Thermogravimetric (TG) analyses were performed in a nitrogen atmosphere to study the thermal stability of samples A2, A3, and A5 (Fig. 5). The TG curve of A2 displays a mass loss of about 21% between 130 °C and 275 °C, probably referring to the desolvation of DMF molecules coordinated to the copper clusters [41]. The presence of coordinated solvent molecules is in agreement with results obtained by FTIR and PXRD techniques. A second mass loss event of 42.4% is observed between 275 °C and 410 °C, probably corresponding to the degradation of the organic ligand [41]. Above 400 °C, there is also a slight loss of 6.1% related to the combustion of leftover organic residues. From 550 °C, no mass loss is observed, suggesting the decomposition of whole

organic matter. XRD analysis of the material after TGA revealed the formation of copper oxide (Fig. S1). The TG curve of the sample A3 obtained at the current of 0.3 A shows three weight losses at 130 °C–250 °C, 250 °C–310 °C, and 310 °C–410 °C. The first step of decomposition (around 11%) may be connected with the desorption of the water molecules coordinated to the metal sites. The second step may refer to further solvent elimination and initial degradation of the organic ligand. The mass loss of 41.6% observed in the third step corresponds to structural collapse resulting from organic ligand decomposition. From above 450 °C copper oxide formation can be considered. For sample A5, there is a 19.7% mass loss between 240 °C and 330 °C, referring to the elimination of a solvent (presence of water, signaled in the infrared spectrum) coordinated apically in the copper clusters. The mass loss of 36.1% between 330 °C and 415 °C refers to the thermal degradation of the organic fraction of the binder in the material structure, the combustion of which results in copper oxide formation, present from 415 °C.

Sample B3 (9.0 V) was used as a reference for samples produced with constant voltage because it has the same major structure, CuBDC2. It also has the same structure as samples A1 (0.1 A) and A2 (0.2 A). The curve for sample B3 showed a mass loss of 21% between 150 °C and 250 °C, also probably referring to the loss of DMF apically coordinated in copper clusters, similar to sample A2 (0.2 A). There was also a 42% loss of mass between 300 °C and 400 °C, referring to the thermal degradation of the organic binder. Above 400 °C, there was a loss of 7.4% related to

the combustion of organic remnants still present from the oxidation of the binder. After 550 °C, mass loss events are no longer observed, assuming the complete degradation of MOF into copper oxide. The results for the thermal analysis of samples A2 and B3 are shown in Fig. S2.

According to the results from elemental analysis samples, A2 and B3 have comparable carbon content (Table S1). The higher the current applied in the synthesis was, the content of carbon was lower (see results for samples A3 and A5), while the content of copper oxide, obtained after TG analysis at 500 °C, was higher. This proves again that the conditions of electrochemical synthesis significantly influence the composition of the resulting materials.

3.5. SEM analysis

The micrographs of the Cu samples (1,4-BDC), synthesized at 0.2 A, 0.4 A, and 9.0 V (samples A2, A5, and B3, respectively), are shown in Fig. 6. All samples present a morphology in the form of agglomerates of irregular shape and diameter. Samples A2 and B3, being a mixture of two phases, appear as plate-like particles with an average size of 304 and 506 nm, respectively (Figs. S3a and c). In the case of sample A5 determined as a pure CuBDC1 phase, crystallites of rod shape are predominant with smaller than for materials A2 and B3 average size (146 nm) (Fig. S3b).
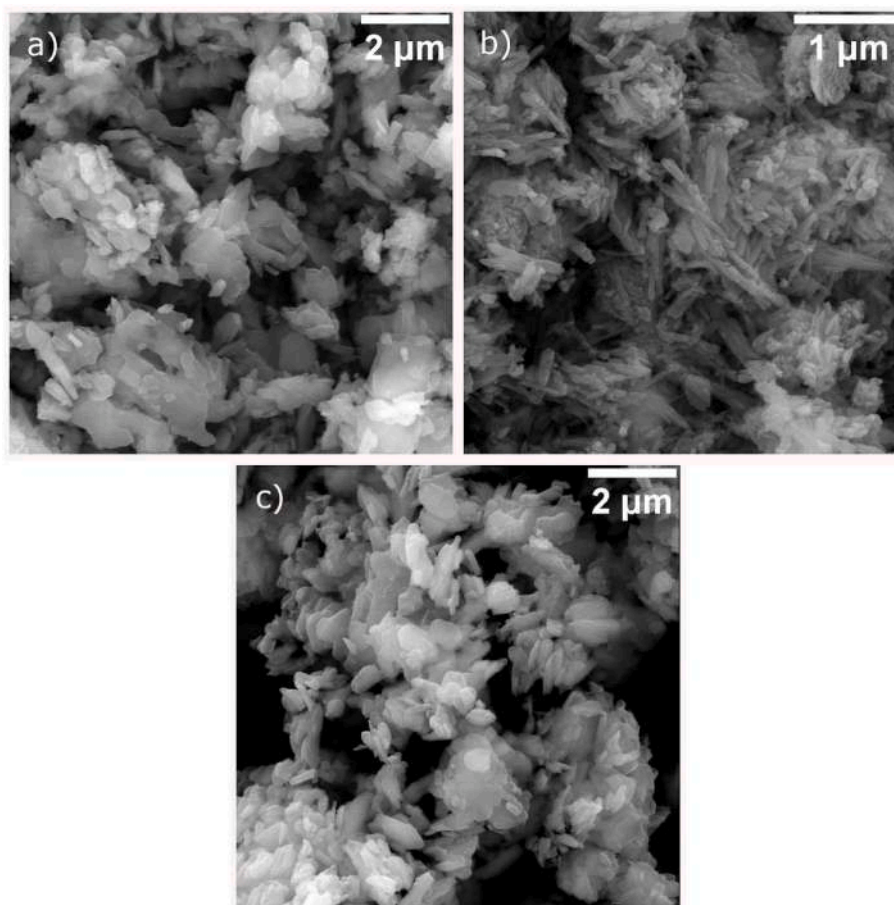

Fig. 6. SEM photographs of samples a) A2 (0.2 A) (mag. 20 000x, scale 2 μm), b) A5 (0.4 A) (mag. 50 000x, scale 1 μm), (c) B3 (9.0 V) (mag. 20 000x, scale 2 μm).

3.6. BET surface area analysis

The surface area analysis performed for sample A5 revealed that the material shows a reversible Type-II isotherm of N_2 sorption/desorption, typical for macroporous sorbents (Fig. S4) [42]. The BET (BJH) surface area of the material was determined as 33.44 (24.96) m^2/g. In comparison with the material obtained in solvothermal (969 m^2/g [41]) and microwave-assisted (374.3 m^2/g [43]) method, this value is low. The dried A5 sample is of porous nature with an average pore diameter of 8.41 nm and cumulative desorption pore volume (BJH method) of 0.13 cc/g.

3.7. Adsorption studies

Sorption experiments were performed for the A5 sample being a pure CuBDC1 phase. As a model pollutant, methylene blue was chosen, which due to its ionic structure, may be adsorbed by BDC-based system via electrostatic interactions. Several parameters such as pH, the sorbent dosage, the dye concentration, temperature, and the contact time were tested to determine their influence on sorption efficiency.

3.7.1. Influence of pH

The initial pH of a pollutant solution is an important parameter in the adsorption process. For this reason, the adsorbed amounts of MB were evaluated in relation to the pH values (fixed by the addition of HCl or NaOH solution) to verify the highest adsorption efficiency of the Cu-based MOF. The results of the 14-h tests are shown in Fig. 7. It can be concluded that the variation in the dye uptakes in the pH range 5–6 were relatively small. The best result equal to 75.91 µmol of the dye adsorbed at 1 g of the MOF was achieved at a pH of 5.56, which is the value of aqueous MB solution without adding HCl or NaOH solution. In more acidic conditions (pH = 4), the sorption efficiency decreased by around 40%, which may be a consequence of the competitive action of H^+ ions with MB molecules for the MOF channels. As these channels have a high negative density, there is greater interaction with positively charged species, such as $H^{+,}$ than with much larger organic cations of the dye. Another reason for the adsorption efficiency drop in acidic conditions may be the decrease of MB cationic form concentration. Under such conditions, the dye also exists as undissociated molecules (50% present
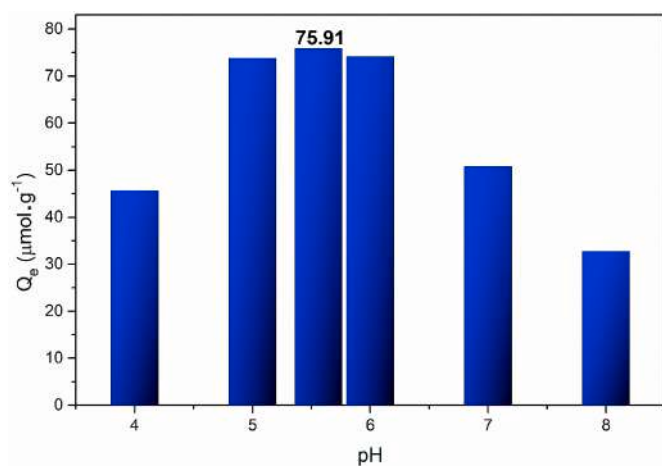
in the solution species at pH ∼ 4) [44]. At a lower pH value, the concentration of undissociated species increases; thus, lower uptake of the pollutant should be expected.

The increased concentration of NaOH in the system negatively influenced the sorption efficiency. At pH 7, the amount of adsorbed dye was determined as 50.81 µmol g^{-1}. The explanation for this can be the electrostatic interactions between Na^+ cations and aromatic rings of the MOF organic linker that may disturb the sorption process of MB. Similar results were reported for the MB removal by HKUST-1 system [17].

3.7.2. Effect of the sorbent mass

The adsorption of cationic dye was studied by changing the quantity of the sorbent while maintaining the initial MB concentration (100 mg L^{-1}). As shown in Fig. 8, the sorption efficiency increased with the increasing mass of the MOF adsorbent. The maximum amount of MB adsorbed under measurement conditions was achieved when 50 mg of the adsorbent was used. A decrease in the sorption effectiveness was noticed for the higher amount of the adsorbent (100 mg). It can be connected with overlapping or aggregation of active sites [45].
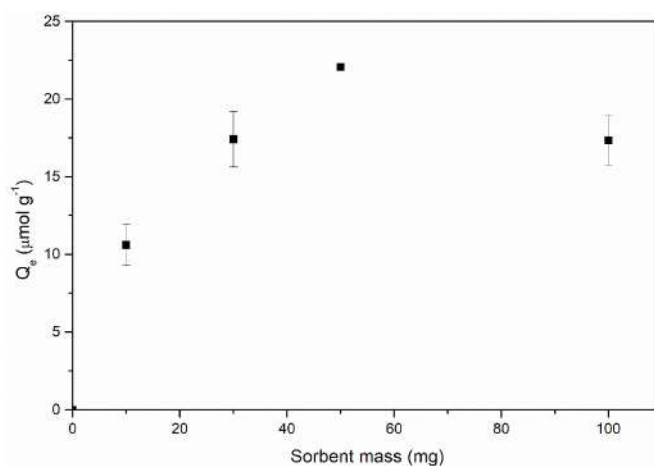
Fig. 8. Effect of the sorbent mass on methylene blue removal by CuBDC1 (c = 100 mg L^{-1}, V = 20.0 mL, T = 20 °C, t = 5 h, pH = 5.5).

Fig. 7. Influence of pH on the removal of methylene blue by sorbent CuBDC1 (250 mg L^{-1}, V = 20.0 mL, m = 30.0 mg, T = 20 °C, t = 14 h). (For interpretation of the references to color in this figure legend, the reader is referred to the Web version of this article.)

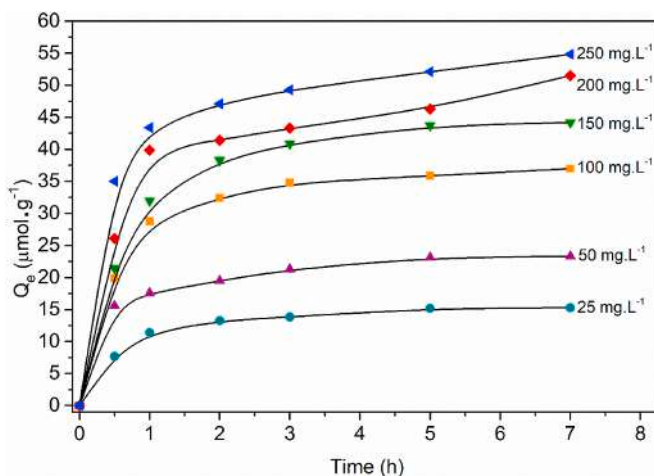**Fig. 9.** Curves of methylene blue adsorption as a function of time at different initial dye concentrations (V = 50.0 mL, T = 20 °C, pH = 5.5). (For interpretation of the references to color in this figure legend, the reader is referred to the Web version of this article.)
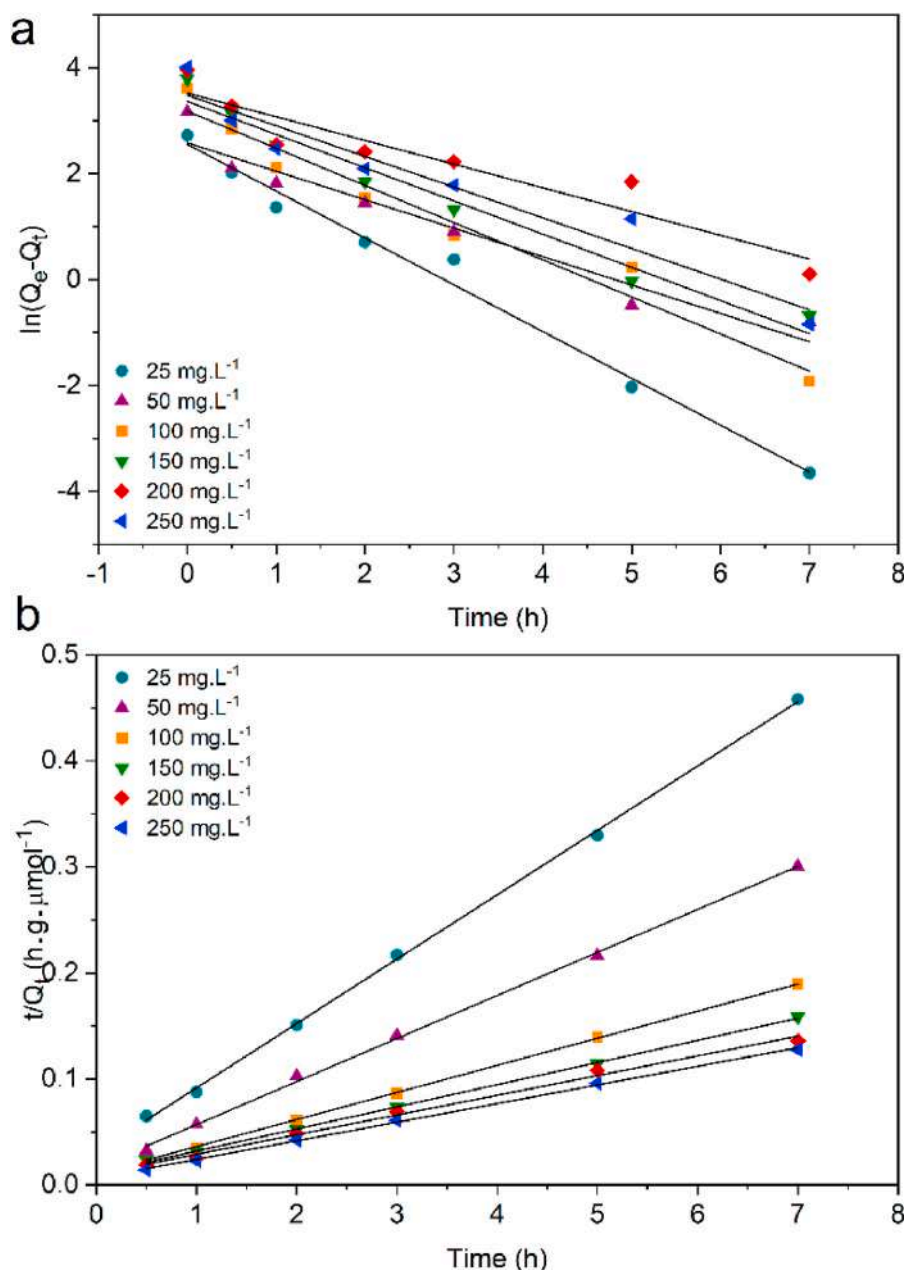
Fig. 10. Fit of a) the pseudo-first, b) pseudo-second-order kinetic models to the experimental data.

3.7.3. Effect of the contact time and adsorption kinetics

To determine the suitable time of contact between MB and the sorbent, a set of experiments at pH 5.5 and a temperature of 293.15 K (20 °C) was carried out (Fig. 9). In the 25–150 mg L^{-1} concentration range of MB solution, the equilibrium was reached after 5 h of the phases contact. For higher concentrations, i.e., 200 and 250 mg L^{-1}, the system did not reach equilibrium even after 7 h. The maximum amounts of the dye adsorbed under measurement conditions were 15.27 and 54.83 µmol g^{-1} for the lowest (i.e., 25 mg L^{-1}) and the highest (250 mg L^{-1}) initial concentration of the adsorbate, respectively. In the first hour of the experiment, adsorption efficiency increased significantly in the case of all tested MB concentrations. This is because at the initial stage of sorption, many active sites are available for the dye molecules; however, upon extending the time, more and more adsorption sites are occupied. This leads to a slower sorption rate and finally reaching equilibrium of the process.

For the evaluation of the kinetics of the sorption process, three

Table 1
Kinetic parameters obtained after fitting the pseudo-second model to the experimental data (c_{MB} = 250 mg L^{-1}).

Parameter	293.15 K	303.15 K	313.15 K
Q_e (µmol g^{-1})	56.818	53.191	46.729
R^2	0.999	0.998	0.999
k_2 (g µmol^{-1} h^{-1})	0.047	0.045	0.056
E_a (kJ mol^{-1})	+8.035		
A (g µmol^{-1} h^{-1})	1.451		
h (µmol g^{-1} h^{-1})	184.012	155.611	148.485
$t_{1/2}$ (h)	0.309	0.342	0.315

models were applied, i.e., the pseudo-first, pseudo-second-order kinetic models, as well as the intraparticle diffusion model. The plots obtained after fitting the pseudo-first and pseudo-second-order model to the experimental data are shown in Fig. 10. In the whole tested concentration range of MB solutions, better fit was obtained for pseudo-second

Table 2

Parameters of the intraparticle diffusion model obtained for adsorption of MB by CuBDC1 at different initial concentrations of the dye.

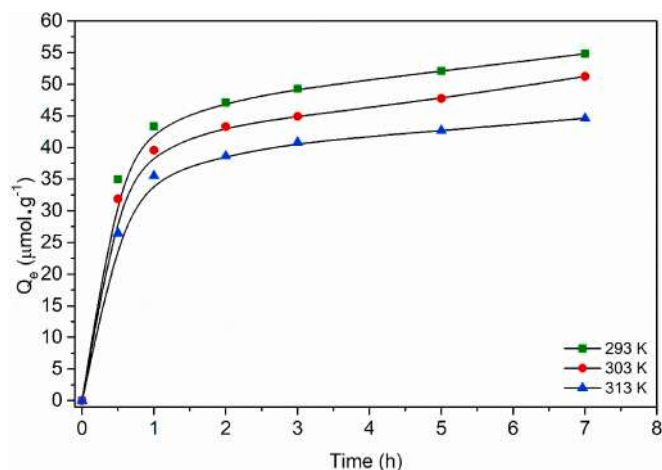| Concentration (mg L^{-1})	k_i (µmol g^{-1} h$^{-0.5}$)	C (µmol g^{-1})	R^2
25	2.960	8.691	0.958
50	4.109	13.390	0.936
100	4.745	25.204	0.870
150	4.820	32.112	0.883
200	5.266	34.330	0.984
250	6.151	38.500	0.998

Fig. 11. Effect of temperature on sorption of MB (c = 250 mg L^{-1}).

than for the pseudo-first-order model (Table S2), which suggests that in MB uptake, complexation of the ionic dye via intramolecular interactions takes place [46]. Similar findings were described for other MB – MOF systems [17,20,22]. Paimam et al. [47] proposed that in MB - MIL-101 system, electrostatic and π-π interactions next to the pore-filling mechanism are responsible for the sorption phenomenon. Kinetic parameters calculated for this model are presented in Table 1. The theoretical value of Q$_e$ is similar to the experimental one (56.82 vs. 54.84 µmol g^{-1}), which proves the adequacy of the model to the experimental results. The half-life time is close to 0.3 h, that is, slightly above 20 min, which means that after this time, the adsorption reaches half of the adsorption capacity from the kinetic point of view. This implies that in the first 30 min of the reaction, possibly at least half of the pores of the material may already be saturated or partially saturated. Haque et al. [20] reported rate constant value $k_2 = 1.83 \times 10^{-3}$ g µmol^{-1} h^{-1} determined for MB concentration equal to 20 mg L^{-1} at 298.15 K. The value obtained by us for a little higher concentration, i.e., 25 mg L^{-1} at 293.15 K was around 26 times higher. Although the experimental conditions were not identical, it can be suspected that our material ensures faster sorption of MB.

Because adsorption is a multi-step process, the intraparticle diffusion model was also considered. The plots shown in Fig. S5 obtained for concentrations higher than 50 mg L^{-1} present multilinearity, which points out that two steps occurred in the sorption process. The first step may be connected with surface adsorption and external diffusion, while the second with gradual adsorption, where intraparticle diffusion is rate-controlling [45]. The analysis of presented rate constants (Table 2) corresponding to intraparticle diffusion shows that the value increased with the increasing initial concentration of the dye. The determined correlation coefficients are in the range 0.870–0.998, which indicates a good model fit to the experimental data. However, in all cases, the intercept C is not equal to zero, which means that the intraparticle diffusion may influence the sorption kinetics, but it is not the only rate-controlling step of the process.
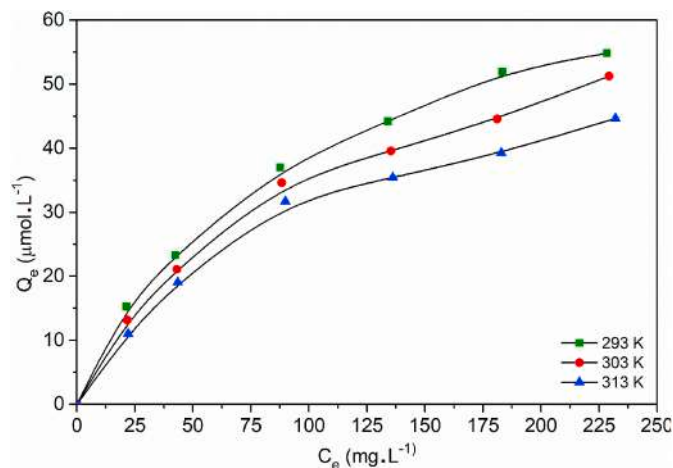

Fig. 12. Adsorption isotherms at different temperatures.

To indicate the effect of temperature on the kinetics of MB sorption by CuBDC1, the experiments for the highest used MB concentration (250 mg L^{-1}) were carried out at three temperatures: 293.15, 303.15, and 313.15 K (Fig. 11). As shown in Table 1, the increased temperature slowed down the initial sorption rate (h). The increase of temperature by 20 K caused the decrease of the sorption rate by around 20%. Moreover, the drop of sorption capacity was observed under higher temperature conditions. At 313.15 K, the Q$_e$ value was lower by c.a. 10 units compared to the value determined at 293.15 K. Similar findings were described for the sorption of MB by HKUST-1, which was determined as an exothermic process [17,48].

3.7.4. Adsorption equilibrium

The analysis of sorption properties is of great importance for the understanding of the mechanisms and the equilibrium of the process. To investigate this the MB-Cu BDC1 system was studied under non-equilibrium conditions in order to observe saturation of the metallurgical network and obtain a maximum adsorption capacity of this material for the dye. As shown in Fig. 12 the sorption capacity increased with the increasing MB initial concentration, however the higher the temperature of the process was, the less dye molecules were adsorbed by 1 g of the sorption material. This temperature-induced effect may be a consequence of shifting of the surface reaction towards the desorption path.

The Langmuir and Freundlich isotherm models were applied to investigate the isothermal data. The fitted curves and determined parameters of both models are presented in Fig. 13 and Table 3. A better fit at all three tested temperatures to the experimental data was observed for Langmuir than for Freundlich isotherm. The application of non-linear equations of the models also proved better compatibility of the Langmuir isotherm to the obtained data (Fig. S6). This suggests that upon MB sorption, a monolayer is created and that the active sites of the CuBDC1 are energetically identical. The values of the R$_L$ parameter are between 0.27 and 0.29, indicating that adsorption is a favorable and reversible process and that it is facilitated by the lowering of temperature.

The maximum sorption capacity at 293.15 K was determined as 76.63 µmol g^{-1}. This value is much higher than the results for HKUST-1 described by Lin et al. [17] (Q$_m$ = 15.28 µmol g^{-1} determined at 298 K) but almost 8 and 6 times lower than the finding reported for MOF-235 [20] (Table 4). However, it should be kept in mind that the process described by us was much faster than for iron terephthalate, as mentioned in the previous paragraph. Considering the results reported in the literature described here, CuBDC1 shows good, however, not excellent efficiency in MB removal from aqueous solutions.

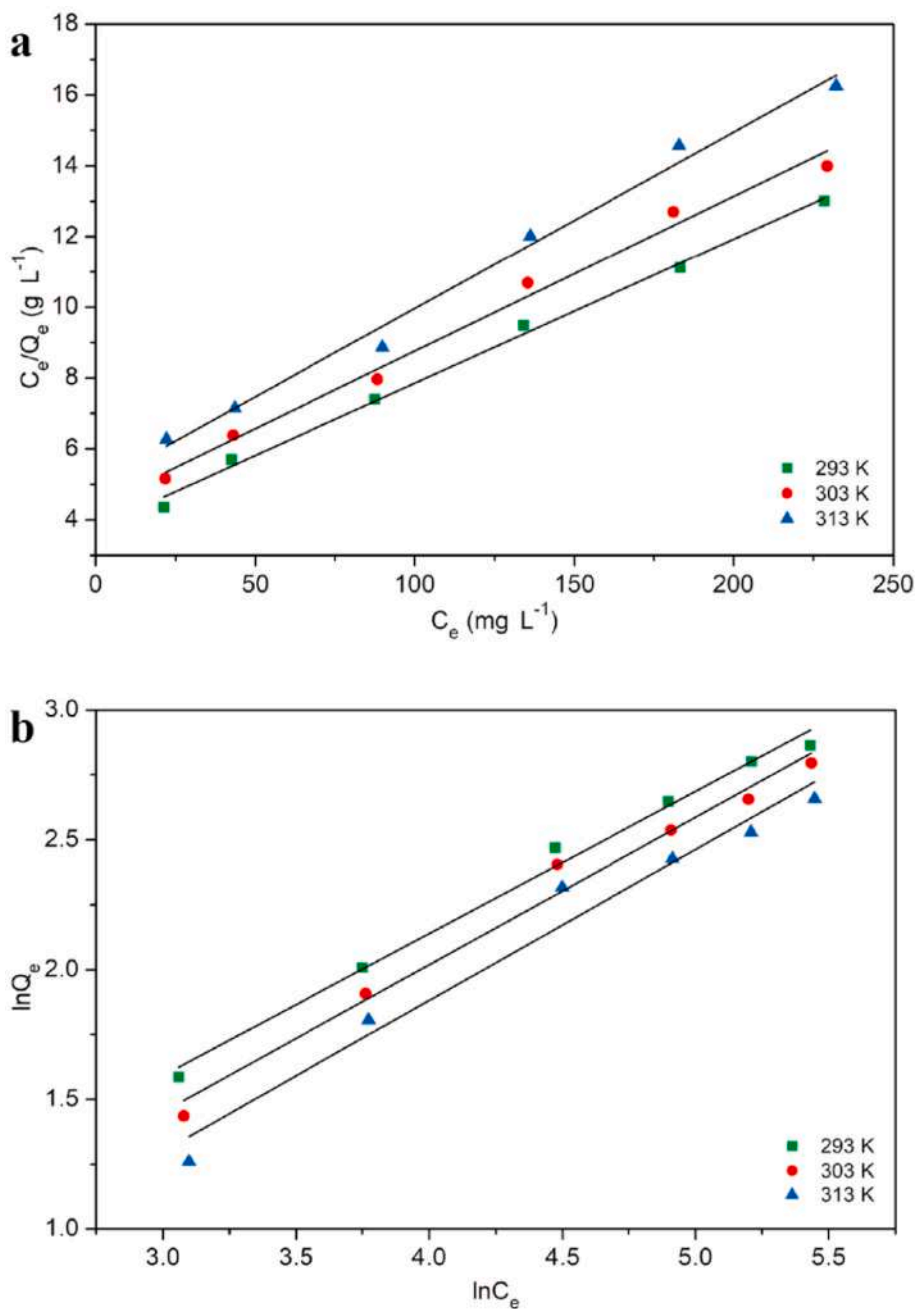The determined K$_L$ values at different temperatures were used to

Fig. 13. The fit of a) Langmuir b) Freundlich isotherm model to the experimental data of MB sorption by CuBDC1.

Table 3
The isotherm parameters for the adsorption of MB on CuBDC1.

| Model	Parameter	Temperature (K)		
		293.15	303.15	313.15
Langmuir	Q_m ($\mu mol\ g^{-1}$)	76.63	71.38	62.65
	K_L (L/mol)	3454.38	3204.90	3195.30
	R_L	0.27	0.28	0.29
	R^2	0.996	0.990	0.991
Freundlich	K_F ($\mu mol\ g^{-1}$)	2.976	2.432	2.010
	n	1.827	1.762	1.721
	R^2	0.992	0.985	0.971

Table 4
Comparison of the maximum sorption capacities (Q_m) and rate constant values (k_2) reported in the literature for MB removal by MOF sorbents.

Sorbent	Q_m ($\mu mol\ g^{-1}$)	T (K)	k_2 ($g\ \mu mol^{-1}\ h^{-1}$)	Reference
Cu(1,4BDC)	76.63	293.15	4.7×10^{-2}	this work
Cu(1,3,5BTC)	15.28	298.15	8.14×10^{-1}	[17]
Cu(1,3,5BTC)	316	298.15	1.34	[48]
Ca(1,4BDC)	83.33	293.15	6.2×10^{-2}	[49]
CoFe(1,4BDC)	9.25	303.15	6.2×10^{-2}	[50]
Cr(1,4 BDC)	26.20	298.15	2.69×10^{-1}	[51]
Fe(1,4BDC)	584.65	298.15	1.83×10^{-3}	[20]
Fe(1,4BDC)	466.62	298.15	2.07×10^{-3}	[47]

Table 5
The thermodynamic parameters of MB sorption on CuBDC1.

Temperature (K)	ΔG (kJ mol^{-1})	ΔH (kJ mol^{-1})	ΔS (J mol^{-1})
293.15	−19.86	−2.98	+57.50
303.15	−20.35		
313.15	−21.01		
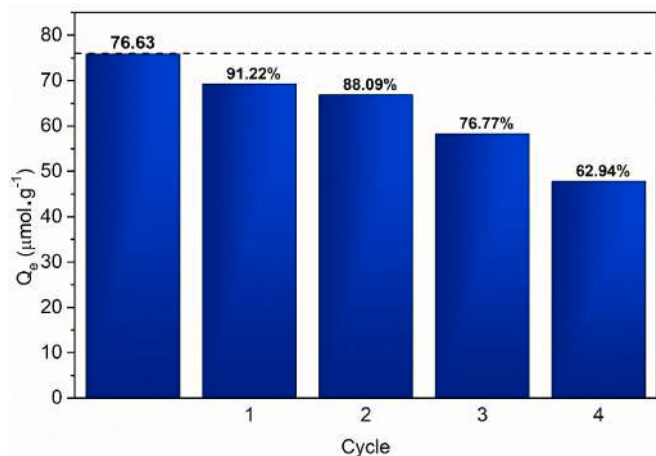
Fig. 14. The effectiveness of MB sorption (c = 250 mg L^{-1}, V = 20.0 mL, m = 40 mg, T = 20 °C, t = 14 h) by CuBDC1 after consecutive regeneration cycles.

investigate the thermodynamic states of the MB sorption process by CuBDC1. The calculated values are presented in Table 5. At all tested temperatures, the determined change of Gibbs free energy has a negative value, which indicates that the dye sorption is a spontaneous process. The negative value of enthalpy change indicates an exothermic reaction, which explains the decrease in sorption capacity upon increasing temperature. Taking into account the energetic range of this value, physisorption of MB by CuBDC1 can be considered where non-covalent intermolecular interactions participate. The positive entropy change implies the increase in randomness, which can be connected with the desorption of the water molecules of the MOF channels. Consequently, the degree of freedom of the water molecules increases, which is probably greater than the decrease in the entropy upon adsorption of the dye molecules in the channels. Thus, the overall entropy of the process increases [21,52].

3.7.5. Regeneration, reusability, stability of the sorption material and utilization in real water sample

The ability to regenerate and reuse a sorbent is an essential issue for industrial practice due to economic and environmental aspects. Thus, sequential MB sorption - desorption experiments were carried out (Fig. 14). In contrast to the destructive and energy-consuming regeneration of activated carbons [53,54], the MOF sorbent can be regenerated by soaking in ethanol at ambient temperature. Although the decrease in the dye sorption capacity was observed in every consecutive cycle, the sorbent could be regenerated and reused four times to ensure satisfactory MB removal from the aqueous solution (Q$_e$ at the third stage of the experiment equals 76.77% of the initial sorption efficiency). In the fourth cycle, the efficiency dropped to 62.94%. It is important to indicate that ethanol used for regeneration can be easily separated from the dye by distillation and recirculated to the regeneration step.

The FTIR spectra of the materials, synthesized, with adsorbed MB, and recycled sorbent, show no significant changes after regeneration (Fig. S7). The position and shape of the absorption bands of CuBDC1 remain the same after the dye desorption, which indicates the material stability during the regeneration process. Also, the SEM analysis indicates no significant changes of the morphology of the CuBDC1 sample

after the dye adsorption (Fig. S9).

To assess the influence of pH on the stability of MOF, the material was soaked in HCl and NaOH solutions for 14 h. After this time, the change of sorbent color at pH 12 was observed (from blue to brown), most probably due to the MOF collapse. Some visual changes were also observed in the system under strongly acidic conditions. In the UV–Vis spectrum of the solution of pH 2, recorded after the phase separation, a new band at around 800 nm was noticed, suggesting that the material is not stable under these conditions (Fig. S8).

To evaluate the potential of CuBDC1 in the treatment of effluents containing MB, the sorption process was carried out with the utilization of water from a natural reservoir. The sorption efficiency for experiments carried out under real-water conditions was surprisingly higher than for the tests performed in distilled water (Q$_e$: 33.6 vs. 22.1 μmol g^{-1}). One possible explanation of these results can be the presence in water from natural reservoirs of substances that enhance interactions of a sorbent with a pollutant. Abate et al. [55] described the positive influence of humic acids on the sorption ability of clay-rich soils. As humic acids are a naturally occurring mixture of macromolecules containing many functional groups like hydroxyl, carboxyl, and carbonyl [56], they may interact with the sorbent and thus offer additional binding sites on its surface [57].

3.7.6. Proposed mechanism of sorption

Considering the molecular structure of MB and CuBDC, the sorption process can be explained by the involvement of electrostatic interactions between the cationic dye and the MOF. Although observed in FTIR spectra, changes after adsorption of MB are very subtle; a widening and a change in the relative intensity of the bands in the range 1600–1400 cm^{-1} (corresponding to vibrations of C=O carboxylic groups) can be observed (Fig. S7).

4. Conclusions

In this study, the 2D Cu(1,4BDC) material was successfully obtained by the electrochemical synthesis in a much shorter time than the conventional solvothermal method. The type of crystal structure and morphology of the resulting product could be controlled by changing the electric current among synthesis protocols. Above 0.35 A, the crystallization of the CuBDC1 phase was favored, in which water molecules are coordinated apically in the copper clusters. The cationic dye – methylene blue was chosen as a model adsorbate in adsorption studies. Although the BET surface area of the material was much lower than described in the literature CuBDC synthesized by solvothermal method, the obtained results showed that the dye could be effectively removed from aqueous solutions under slightly acidic conditions (pH 5–6) at a temperature of 293.15 K. The kinetic and isotherms experiments carried out at three temperatures indicated that the adsorption of MB takes place at a relatively homogeneous surface and that the rate-controlling step of this spontaneous and exothermic process is a complexation phenomenon, in which electrostatic and π-π interactions may play a major role. The isothermal adsorption data were fitted well by the Langmuir model showing a maximum sorption capacity of 76.63 μmol g^{-1}. After dye sorption, MOF could be easily regenerated under mild conditions and reused three times without a drastic decrease in sorption efficiency (76.77% of sorption ability after the fourth cycle). The results also showed the structural stability of the sorbent in the best uptake conditions.

CRediT authorship contribution statement

Arthur Felipe de Farias Monteiro: Data curation, Formal analysis, Investigation, Methodology, Visualization, Writing – original draft, Writing – review & editing. **Stephany Larissa da Silva Ribeiro:** Formal analysis. **Thiago Izidoro Silva Santos:** Formal analysis. **José Daniel da Silva Fonseca:** Writing – review & editing, Writing – original draft,

Visualization, Formal analysis, Data curation. **Natalia Łukasik:** Formal analysis, Writing – original draft, Writing – review & editing. **Joanna Kulesza:** Writing – review & editing, Writing – original draft, Supervision, Methodology, Investigation, Data curation, Conceptualization. **Bráulio Silva Barros:** Writing – review & editing, Writing – original draft, Visualization, Supervision, Resources, Software, Funding acquisition, Formal analysis, Conceptualization.

Declaration of competing interest

The authors declare that they have no known competing financial interests or personal relationships that could have appeared to influence the work reported in this paper.

Acknowledgments

Appendix A. Supplementary data

Supplementary data to this article can be found online at https://doi.org/10.1016/j.micromeso.2022.111938.

References

[1] J. Duan, S. Chen, C. Zhao, Ultrathin metal-organic framework array for efficient electrocatalytic water splitting, Nat. Commun. 8 (2017) 15341, https://doi.org/10.1038/ncomms15341.

[2] Y. Wang, M. Zhao, J. Ping, B. Chen, X. Cao, Y. Huang, C. Tan, Q. Ma, S. Wu, Y. Yu, Q. Lu, J. Chen, W. Zhao, Y. Ying, H. Zhang, Bioinspired design of ultrathin 2D bimetallic metal-organic-framework nanosheets used as biomimetic enzymes, Adv. Mater. 28 (2016) 4149–4155, https://doi.org/10.1002/adma.201600108.

[3] A.C. de Oliveira Frós, M.A. de Oliveira, A.A. Macêdo Soares, F. Hallwass, J. Chojnacki, B.S. Barros, S.A. Júnior, J. Kulesza, Selective adsorption of BTEX on calixarene-based molecular coordination network determined by 13C NMR spectroscopy, Inorg. Chim. Acta. 492 (2019) 161–166, https://doi.org/10.1016/j.ica.2019.04.031.

[4] T. Rodenas, I. Luz, G. Prieto, B. Seoane, H. Miro, A. Corma, F. Kapteijn, F.X. Llabrés i Xamena, J. Gascon, Metal–organic framework nanosheets in polymer composite materials for gas separation, Nat. Mater. 14 (2015) 48–55, https://doi.org/10.1038/nmat4113.

[5] G. Gumilar, Y.V. Kaneti, J. Henzie, S. Chatterjee, J. Na, B. Yuliarto, N. Nugraha, A. Patah, A. Bhaumik, Y. Yamauchi, General synthesis of hierarchical sheet/plate-like M-BDC (M = Cu, Mn, Ni, and Zr) metal–organic frameworks for electrochemical non-enzymatic glucose sensing, Chem. Sci. 11 (2020) 3644–3655, https://doi.org/10.1039/C9SC05636J.

[6] N. Ahmad, H.A. Younus, A.H. Chughtai, K. Van Hecke, Z.A.K. Khattak, Z. Gaoke, M. Danish, F. Verpoort, Synthesis of 2D MOF having potential for efficient dye adsorption and catalytic applications, Catal. Sci. Technol. 8 (2018) 4010–4017, https://doi.org/10.1039/c8cy00579f.

[7] R.-Q. Zhong, R.-Q. Zou, Q. Xu, Solvent-induced deviation in square-grid layers of microporous Cu(II) isophthalates: layer stacking and gas adsorption properties, CrystEngComm 13 (2011) 577–584, https://doi.org/10.1039/C0CE00150C.

[8] G. Zhan, L. Fan, F. Zhao, Z. Huang, B. Chen, X. Yang, S. Zhou, Fabrication of ultrathin 2D Cu-BDC nanosheets and the derived integrated MOF nanocomposites, Adv. Funct. Mater. 29 (2019) 1806720, https://doi.org/10.1002/adfm.201806720.

[9] H. Li, M. Eddaoudi, T.L. Groy, O.M. Yaghi, Establishing microporosity in open Metal–Organic frameworks: gas sorption isotherms for Zn(BDC) (BDC = 1,4-benzenedicarboxylate), J. Am. Chem. Soc. 120 (1998) 8571–8572, https://doi.org/10.1021/ja981669x.

[10] C.G. Carson, K. Hardcastle, J. Schwartz, X. Liu, C. Hoffmann, R.A. Gerhardt, R. Tannenbaum, Synthesis and structure characterization of copper terephthalate metal-organic frameworks, Eur. J. Inorg. Chem. (2009) 2338–2343, https://doi.org/10.1002/ejic.200801224, 2009.

[11] H.F. Clausen, R.D. Poulsen, A.D. Bond, M.-A.S. Chevallier, B.B. Iversen, Solvothermal synthesis of new metal organic framework structures in the zinc–terephthalic acid–dimethyl formamide system, J. Solid State Chem. 178 (2005) 3342–3351, https://doi.org/10.1016/j.jssc.2005.08.013.

[12] J. Liu, B. Lukose, O. Shekhah, H.K. Arslan, P. Weidler, H. Gliemann, S. Bräse, S. Grosjean, A. Godt, X. Feng, K. Müllen, I.-B. Magdau, T. Heine, C. Wöll, A novel series of isoreticular metal organic frameworks: realizing metastable structures by liquid phase epitaxy, Sci. Rep. 2 (2012) 921, https://doi.org/10.1038/srep00921.

[13] V.S.G. Garcia, L. de Freitas Tallarico, J.M. Rosa, C.F. Suzuki, D.A. Roubicek, E. Nakano, S.I. Borrely, Multiple adverse effects of textile effluents and reactive Red 239 dye to aquatic organisms, Environ. Sci. Pollut. Res. 28 (2021) 63202–63214, https://doi.org/10.1007/s11356-021-15115-7.

[14] J. Sharma, S. Sharma, V. Soni, Classification and impact of synthetic textile dyes on Aquatic Flora: a review, Reg. Stud. Mar. Sci. 45 (2021), https://doi.org/10.1016/j.rsma.2021.101802.

[15] M. Yadav, M. Das, C. Savani, S. Thakore, R. Jadeja, Maleic anhydride cross-linked β-cyclodextrin-conjugated magnetic nanoadsorbent: an ecofriendly approach for simultaneous adsorption of hydrophilic and hydrophobic dyes, ACS Omega 4 (2019) 11993–12003, https://doi.org/10.1021/acsomega.9b00881.

[16] Z. Singh, P. Chadha, Textile industry and occupational cancer, J. Occup. Med. Toxicol. 11 (2016) 1–6, https://doi.org/10.1186/s12995-016-0128-3.

[17] S. Lin, Z. Song, G. Che, A. Ren, P. Li, C. Liu, J. Zhang, Adsorption behavior of metal–organic frameworks for methylene blue from aqueous solution, Microporous Mesoporous Mater. 193 (2014) 27–34, https://doi.org/10.1016/j.micromeso.2014.03.004.

[18] M. Xiaobo, L. Xinyu, Z. Jie, H. Xiaoxian, Y. Weichun, Heterostructured TiO 2 @ HKUST-1 for the enhanced removal of methylene blue by integrated adsorption and photocatalytic degradation, Environ. Technol. 42 (2021) 4134–4144, https://doi.org/10.1080/09593330.2020.1745295.

[19] I. Mantasha, H.A.M. Saleh, K.M.A. Qasem, M. Shahid, M. Mehtab, M. Ahmad, Efficient and selective adsorption and separation of methylene blue (MB) from mixture of dyes in aqueous environment employing a Cu(II) based metal organic framework, Inorg. Chim. Acta. 511 (2020), https://doi.org/10.1016/j.ica.2020.119787, 119787.

[20] E. Haque, J.W. Jun, S.H. Jhung, Adsorptive removal of methyl orange and methylene blue from aqueous solution with a metal-organic framework material, iron terephthalate (MOF-235), J. Hazard Mater. 185 (2011) 507–511, https://doi.org/10.1016/j.jhazmat.2010.09.035.

[21] C. Chen, M. Zhang, Q. Guan, W. Li, Kinetic and thermodynamic studies on the adsorption of xylenol orange onto MIL-101(Cr), Chem. Eng. J. 183 (2012) 60–67, https://doi.org/10.1016/j.cej.2011.12.021.

[22] V.K.-M. Au, Y. Kwan, N. Lai, K. Low, Dual-functional mesoporous copper (II) metal-organic frameworks for the remediation of organic dyes, Chem. Eur J. 27 (2021) 9174–9179, https://doi.org/10.1002/chem.202100289.

[23] A. Martinez Joaristi, J. Juan-Alcañiz, P. Serra-Crespo, F. Kapteijn, J. Gascon, Electrochemical synthesis of some archetypical Zn 2+ , Cu 2+ , and Al 3+ metal organic frameworks, Cryst. Growth Des. 12 (2012) 3489–3498, https://doi.org/10.1021/cg300552w.

[24] The Cambridge crystallographic data centre, Mercury (n.d.), https://www.ccdc.cam.ac.uk/Community/csd-community/freemercury/.

[25] H. Putz, K. Brandenburg, Diamond- crystal and molecular structure visualization (n.d.), https://www.crystalimpact.de/diamond.

[26] S. Lagergren, About the theory of so-called adsorption of soluble substances, K. - Sven. Vetenskapsakademiens Handl. 24 (1898) 1–39.

[27] Y.S. Ho, G. McKay, Kinetic models for the sorption of dye from aqueous solution by wood, Process Saf. Environ. Protect. 76 (1998) 183–191, https://doi.org/10.1205/095758298529326.

[28] W.J. Weber, J.C. Morris, Kinetics of adsorption on carbon from solution, J. Sanit. Eng. Div. 89 (1963) 31–60.

[29] I. Langmuir, The adsorption of gases on plane surfaces of glass, mica and platinum, J. Am. Chem. Soc. 40 (1919) 1361–1403, https://doi.org/10.1021/ja02242a004.

[30] A. Afkhami, T. Madrakian, A. Amini, Mo(VI) and W(VI) removal from water samples by acid-treated high area carbon cloth, Desalination 243 (2009) 258–264, https://doi.org/10.1016/j.desal.2008.04.028.

[31] H. Freundlich, W. Heller, The adsorption of cis- and trans-azobenzene, J. Am. Chem. Soc. 61 (1939) 2228–2230, https://doi.org/10.1021/ja01877a071.

[32] R. Seetharaj, P.V. Vandana, P. Arya, S. Mathew, Dependence of solvents, pH, molar ratio and temperature in tuning metal organic framework architecture, Arab. J. Chem. 12 (2019) 295–315, https://doi.org/10.1016/j.arabjc.2016.01.003.

[33] X.Q. Lu, J.J. Jiang, C.L. Chen, B.S. Kang, C.Y. Su, 3D coordination polymers with nitrilotriacetic and 4,4′-bipyridyl mixed ligands: structural variation based on dinuclear or tetranuclear subunits assisted by Na-O and/or O-H···O interactions, Inorg. Chem. 44 (2005) 4515–4521, https://doi.org/10.1021/ic050125a.

[34] H.Y. Bai, W.Q. Fan, C.B. Liu, W.D. Shi, Y.S. Yan, synthesis, Structure and electrochemical behavior of a 3D crystalline copper(II) metal-organic framework, Funct. Mater. Lett. 7 (2014) 4–7, https://doi.org/10.1142/S1793604714500490.

[35] N.E. Tari, A. Tadjarodi, J. Tamnanloo, S. Fatemi, Facile and fast, one pot microwave synthesis of metal organic framework copper terephthalate and study CO2 and CH4 adsorption on it, J. Porous Mater. 22 (2015) 1161–1169, https://doi.org/10.1007/s10934-015-9992-y.

[36] G.B. Deacon, R.J. Phillips, Relationships between the carbon-oxygen stretching frequencies of carboxylato complexes and the type of carboxylate coordination, Coord. Chem. Rev. 33 (1980) 227–250, https://doi.org/10.1016/S0010-8545(00)80455-5.

[37] A. Patra, T.K. Sen, R. Bhattacharyya, S.K. Mandal, M. Bera, Diversity of carboxylate binding in a new tetranuclear zinc cluster: correlation between spectroscopic investigations and carboxylate binding modes, RSC Adv. 2 (2012) 1774–1777, https://doi.org/10.1039/c2ra01317g.

[38] H.K. Arslan, O. Shekhah, D.C.F. Wieland, M. Paulus, C. Sternemann, M.A. Schroer, S. Tiemeyer, M. Tolan, R.A. Fischer, C. Wöll, Intercalation in layered metal-organic frameworks: reversible inclusion of an extended π-system, J. Am. Chem. Soc. 133 (2011) 8158–8161, https://doi.org/10.1021/ja2037996.

[39] O.J. Silva Junior, A.F.F. Monteiro, J.B.L. Oliveira, A.M.U. Araújo, D.G. Silva, J. Kulesza, B.S. Barros, Coordination polymer-derived CuO catalysts for oxidative

degradation of methylene blue, Mater. Chem. Phys. 235 (2019) 121737, https://doi.org/10.1016/j.matchemphys.2019.121737.

[40] Z. Guo, M.V. Reddy, B.M. Goh, A.K.P. San, Q. Bao, K.P. Loh, Electrochemical performance of graphene and copper oxide composites synthesized from a metal–organic framework (Cu-MOF), RSC Adv. 3 (2013) 19051, https://doi.org/10.1039/c3ra43308k.

[41] M. Varmazyari, Y. Khani, F. Bahadoran, Z. Shariatinia, S. Soltanali, Hydrogen production employing Cu(BDC) metal–organic framework support in methanol steam reforming process within monolithic micro-reactors, Int. J. Hydrogen Energy 46 (2021) 565–580, https://doi.org/10.1016/j.ijhydene.2020.09.245.

[42] K.S.W. Sing, D.H. Everett, R.A.W. Haul, L. Moscou, R.A. Pietrotti, J. Rouquerol, T. Siemieniewska, Reporting physisorption data for gas/solid system with special reference to the determination of surface area and porosity, Pure Appl. Chem. 57 (1985) 603–619, https://doi.org/10.1351/pac198557040603.

[43] A. Dastbaz, J. Karimi-Sabet, M.A. Moosavian, Intensification of hydrogen adsorption by novel Cu-BDC@rGO composite material synthesized in a microwave-assisted circular micro-channel, Chem. Eng. Process. - Process Intensif. 135 (2019) 245–257, https://doi.org/10.1016/j.cep.2018.11.004.

[44] J.J. Salazar-Rabago, R. Leyva-Ramos, J. Rivera-Utrilla, R. Ocampo-Perez, F. J. Cerino-Cordova, Biosorption mechanism of Methylene Blue from aqueous solution onto White Pine (Pinus durangensis) sawdust: effect of operating conditions, Sustain. Environ. Res. 27 (2017) 32–40, https://doi.org/10.1016/j.serj.2016.11.009.

[45] G. Crini, H.N. Peindy, F. Gimbert, C. Robert, Removal of C.I. Basic Green 4 (Malachite Green) from aqueous solutions by adsorption using cyclodextrin-based adsorbent: kinetic and equilibrium studies, Separ. Purif. Technol. 53 (2007) 97–110, https://doi.org/10.1016/j.seppur.2006.06.018.

[46] J. Li, X. Wang, G. Zhao, C. Chen, Z. Chai, A. Alsaedi, T. Hayat, X. Wang, Metal-organic framework-based materials: superior adsorbents for the capture of toxic and radioactive metal ions, Chem. Soc. Rev. 47 (2018) 2322–2356, https://doi.org/10.1039/c7cs00543a.

[47] S.H. Paiman, M.A. Rahman, T. Uchikoshi, N. Abdullah, M.H.D. Othman, J. Jaafar, K.H. Abas, A.F. Ismail, Functionalization effect of Fe-type MOF for methylene blue adsorption, J. Saudi Chem. Soc. 24 (2020) 896–905, https://doi.org/10.1016/j.jscs.2020.09.006.

[48] R. Kaur, A. Kaur, A. Umar, W.A. Anderson, S.K. Kansal, Metal organic framework (MOF) porous octahedral nanocrystals of Cu-BTC: synthesis, properties and enhanced absorption properties, Mater. Res. Bull. 109 (2019) 124–133, https://doi.org/10.1016/j.materresbull.2018.07.025.

[49] O.J. Silva Junior, C.V.C. Moreira, A.F. De Farias Monteiro, V.E.R. Melo, J.B. L. Oliveira, J. Kulesza, B.S. Barros, SÍNTESE, CARACTERIZAÇÃO E APLICAÇÃO DE Ca-MOFs NA REMOÇÃO DO AZUL DE METILENO POR ADSORÇÃO, Quim. Nova X (2022) 1–11, https://doi.org/10.21577/0100-4042.20170852.

[50] S. Soni, P.K. Bajpai, J. Mittal, C. Arora, Utilisation of cobalt doped iron based MOF for enhanced removal and recovery of methylene blue dye from waste water, J. Mol. Liq. 314 (2020) 113642, https://doi.org/10.1016/j.molliq.2020.113642.

[51] T. Shen, J. Luo, S. Zhang, X. Luo, Hierarchically mesostructured MIL-101 metal-organic frameworks with different mineralizing agents for adsorptive removal of methyl orange and methylene blue from aqueous solution, J. Environ. Chem. Eng. 3 (2015) 1372–1383, https://doi.org/10.1016/j.jece.2014.12.006.

[52] F. Leng, W. Wang, X.J. Zhao, X.L. Hu, Y.F. Li, Adsorption interaction between a metal-organic framework of chromium-benzenedicarboxylates and uranine in aqueous solution, Colloids Surfaces A Physicochem. Eng. Asp. 441 (2014) 164–169, https://doi.org/10.1016/j.colsurfa.2013.08.074.

[53] Y. Guo, E. Du, The effects of thermal regeneration conditions and inorganic compounds on the characteristics of activated carbon used in power plant, Energy Proc. 17 (2012) 444–449, https://doi.org/10.1016/j.egypro.2012.02.118.

[54] J.E. Park, G.B. Lee, B.U. Hong, S.Y. Hwang, Regeneration of activated carbons spent by waste water treatment using KOH chemical activation, Appl. Sci. 9 (2019), https://doi.org/10.3390/app9235132.

[55] G. Abate, J.C. Penteado, J.D. Cuzzi, G.C. Vitti, J. Lichtig, J.C. Masini, Influence of humic acid on adsorption and desorption of atrazine, hydroxyatrazine, deethylatrazine, and deisopropylatrazine onto a clay-rich soil sample, J. Agric. Food Chem. 52 (2004) 6747–6754, https://doi.org/10.1021/jf049229e.

[56] H.-R. Schulten, M. Schnitzer, A state of the art structural concept for humic substances, Naturwissenschaften 80 (1993) 29–30.

[57] K. Hemine, N. Łukasik, M. Gazda, I. Nowak, B-Cyclodextrin-containing polymer based on renewable cellulose Resources for effective removal of ionic and non-ionic toxic organic pollutants from water, J. Hazard Mater. 418 (2021), https://doi.org/10.1016/j.jhazmat.2021.126286.